Polymer Bulletin
https://doi.org/10.1007/s00289-025-05821-4

ORIGINAL PAPER

Synthesis, characterization, and photophysical properties of innovative polyketone luminophores: exhibiting clustering-triggered emission and metal ion sensing

Marwa M. Sayed[1] · Islam S. Marae[2] · Mohamed F. Mostafa[3] · Kamal I. Aly[4] · Etify A. Bakhite[2]

Received: 16 September 2024 / Revised: 26 February 2025 / Accepted: 2 May 2025

Abstract

Clustering-triggered emission (CTE) luminophores are novel luminescence compounds lacking extensive conjugation and receiving considerable interest. Two novel fluorescent polyketones (PKs) with a styrene unit as a pendant group in their backbone have been successfully synthesized. They are distinguished by the groups that separate the attached repeating monomeric units diacetyl cyclohexanone styrene (DAcSt), polyketone ether styrene (PKESt) with two benzene rings separated by an aliphatic ether or polyketone styrene (PKSt) with a single benzene ring. Using different techniques to investigate the structural, thermal stabilities, and morphological analyses of the polymers (PKSt, PKESt), their photophysical luminescence behavior is examined, and it appears that they are novel CTE compounds as a result of numerous n-π*, π-π* transitions and hydrogen-bonding interaction, displaying aggregation-induced emission (AIE) phenomena. PKESt has excitation-independent emission and generates blue light at different excitation wavelengths even at a short wavelength of 256 nm, while PKSt emits white light at 256 nm and blue emission at 325 nm, showing excitation-dependent wavelength. These unique luminous phenomena will bring light to the mechanism of clusteroluminescence (CL) and provide new approaches to the rational design of innovative luminescent materials. This study not only discloses new properties of PKs clustering emission but also gives novel perspectives on how to use PKs clustering emission to build novel types of luminescence systems. This system's potential is metal ion sensors for transition metals (Zn^{2+}, Ni^{2+}, Co^{2+}, Cu^{2+}, Fe^{3+}) with outstanding selective fluorescence response to Fe^{3+} ions. These polymers may be useful photocatalytic materials with ferric ions since Fe^{3+} ions quench these Pks.

Keywords Clustering-triggered emission (CTE) · Nonconjugated polymer · Clusteroluminescence (CL) fluorescent polyketone · Aggregation-induced emission (AIE) · Metal sensors

Extended author information available on the last page of the article

Published online: 29 May 2025

Introduction

Unconventional methods of producing polymers are being investigated in the dynamic subject of materials science to make groundbreaking discoveries. The most common luminescent polymers often have numerous conjugated π-aromatic building components put into them [1, 2]. Due to their strong emission capabilities, these materials have attracted attention in a wide variety of applications, including organic lasers and organic light-emitting diodes (OLEDs) [3], solar cells [4], sensors [5], bioimaging [6], optoelectronic material [7], and more. However, their more comprehensive application challenges include complex production, toxicity from vast conjugated systems, and photobleaching. These polymers are highly luminous in diluted solutions but display much reduced or no emission in concentrated or aggregated forms due to the aggregation-caused quenching (ACQ) phenomenon [7]. Nonconventional luminous polymers (NLPs) are being studied by scientists as a possible solution to these problems [8, 9]. These materials avoid using large π-conjugated structures to mitigate the disadvantages of traditional luminous polymers. Separated benzene rings, distinct subgroups (-OH, -NH_2, C=C, and C=N), and heteroatoms (N, O, P, and S) are typical features of this novel class of luminous polymers [10–12]. In contrast to other luminophore, their emission has some unique features, as they do not need any delocalized electrons to be excited, and they act as a group of molecules instead of a separated, independent group, which makes them emit a lot of light when they are gathered together [8, 13].

Nonconjugated and nonaromatic heteroatom-based polymers (such as poly(maleic anhydride), natural protein, and synthetic poly(amido amine), exhibit exceptional luminescence that is not explained by extended through-bond conjugation (TBC) theories [14–17]. Since the discovery of "clusteroluminescence (CL)" a new term for it, which denotes the long-wavelength emission occurrence in structures with nonconjugation in a clustering state, scientists have devoted greater attention to this phenomenon [18–20]. Clusteroluminescent polymers have drawn the interest of researchers with their unusual features and possible uses, standing out among the variety of materials competing for attention [21]. These CL structures can be composed of only n-electron CL-based materials, such as polyether, polythioether, and polyamine, or just π-electron CL-based materials with separated aromatic rings, such as diphenylmethane, diphenylethane, polystyrene; and (n, π)-electron hybrid CL-based materials, such as polyketone, polyester, and polyamide, depending on their electronic components.

According to specific theories, a possible source of CL is electron delocalization caused by hydrogen bonds, oxidation of nitrogen atoms [13, 22], and involvement of impurities in nonaromatic polymers, such as synthetic nonconjugated materials like polyester, polyanhydride, and natural ones like starch, and sodium alginate [12, 23]. The recently revealed through-space interactions (TSI) in carbonyl-based structures and nonconjugated hydrocarbon systems have greatly accelerated the development of CL in the last five years [24–28].

Clusteroluminescent polymers have exceptional properties that might be used for metal sensing and could significantly improve metal ion detection efficiency,

sensitivity, and selectivity [21]. Metal sensing is very relevant to many fields in protecting ecosystems and human health [29], and environmental scientists prioritize tracking quantities of heavy metals in water sources [30, 31]. The high expense, lack of flexibility for on-site analysis, and discomfort of frequently used techniques like inductively coupled plasma mass spectrometry (MS) and atomic absorption spectrometry make it challenging to employ these methods for reliable measurements of metal ions [32]. Fluorescent detection technologies are less expensive options that can overcome these restrictions; however, they need to develop and produce highly specialized sensor molecules for each analyte [33].

This study included the synthesis of two new polyketones (PK); both have a styrene unit in their backbone, but they differ in terms of the groups separating the repeating units attached to them (one benzene ring PKSt or two benzene rings separating by aliphatic ether PKESt). Extensive structural and photophysical analysis was performed on the polymers (PKSt, PKESt). The distinct fluorescence responses induced by these PKs and selected metal ions via polymer−metal ion interactions showed unique responses in binding to these metal ions with selectivity toward ferric ions. This research aims to boost the development of sensing systems for future generations and illuminate the approaches to more effective, observant, and particular metal sensing, which will have global impacts.

Experimental

Materials

Acetylacetone, Imidazole, Terephthalaldehyde (Alfa Aesar), 4-Hydroxy benzaldehyde, Potassium Carbonate (K_2CO_3), Cinnamaldehyde (El Nasser chemicals), 1,8-Dichlorooctane (Merck), Ethanol absolute (Alfa Chemicals), Dimethyl Formamide (DMF), Dimethyl sulfoxide (DMSO), Zinc Acetate ($(CH_3COO)_2Zn$), Nickel (II) Sulfate ($NiSO_4$), Hexahydrate Cobalt (II) Chloride ($CoCl_2$), Copper (II) Acetate hydrate ($(CH_3COO)_2Cu$), and Ferric (III) Chloride anhydrous ($FeCl_3$), are received from Sigma-Aldrich and used without passing through any purification processes.

Measurements

An elemental analysis system GmbH, VARIOEL, was used to perform the elemental analyses. Fourier transform infrared spectroscopy (FT-IR) is measured using the KBr technique by Shimadzu 2110 PC scanning spectrometers. Nuclear magnetic resonance (^{1}H-NMR) and ^{13}C-NMR spectra were recorded using deuterated $CDCl_3$ as a solvent using a JEOL (ECA 500) spectrometer. The crystalline nature of the materials is studied utilizing the powdered samples approach and the X-ray diffraction crystallography (XRD) Goniometer PW3050/60 scan type with the XPERT-PRO diffractometer system. The TA Q-600 Thermal Analyzer measures thermogravimetric analysis (TGA) in a nitrogen environment (N_2) at a heating rate of 10 ℃/min. The Shimadzu mini 1240 is used to measure UV–Vis spectra. Hitachi F-7100

FL Spectrophotometer measures fluorescence emission spectra at room temperature. The Hitachi S-4800 scanning electron microscope (SEM) was used to identify the surface morphology of the selected polymers by coating procedure.

Synthesis of 2,4-diacetyl-5-hydroxy-5-methyl-3-styryl cyclohexanone (DAcSt)

A solution of cinnamaldehyde (0.1 mol, 13.2 mg) in DMSO (20 mL) was treated with acetylacetone (0.2 mol, 20 mg) and imidazole as a base catalyst (0.02 mol, 1.36 mg). The solution is stirred at r.t for seven days. Through this period, white crystals grow from the bottom and walls of the reaction pot. The white precipitate is filtered off under a vacuum, washed with water several times, and dried and crystalized by ethanol. Yield: 20%; m.p. 180° C: Elemental Anal. for $C_{19}H_{22}O_4$: Calcd. %: C, 72.59; H, 7.05. Found %: C, 72.05; H, 7.01.^{1}H-NMR ($CDCl_3$, 500 MHz) revealed the bands at δ: 7.22–7.33 (m, 5H, Ar–H); 6.45–6.48 (d, 1H, -CH=CH-); 5.97–6.02 (dd, 1H, -CH=CH-); 5.22 (s, 1H, OH); 3.73–3.75 (d, 1H, C2H); 3.59–3.61 (dd, 1H, C3H); 2.90–2.92 (d, 1H, C4H); 2.77–2.80 (d, 1H, C6H); 2.30–2.33 (d, 1H, C6H); 2.16 (s, 3H, CH_3); 2.08 (s, 3H, CH_3); 2.17 (S, 3H, CH_3). ^{13}C-NMR revealed 16 environments of carbon as expected at δ: 210.34 ppm for (C_a = O), 206.36 ppm for (C_b = O), 205.63 ppm for (C_c = O), (136.84, 132.37, 129.17, 129.12 ppm) for aromatic carbon, (126.70, 72.90, 66.59, 63.65 ppm) for carbons of cyclohexanone, CH_3 of acetyl for (55.65, 42.03 ppm), 28.63 ppm for (-C_o–C = CH) produced from aldehyde condensation.

Synthesis of monomer 4,4-diformyl-α,ω-diphenoxyoctane

The monomer was synthesized according to the procedure described in our previous studies [34–36]**.**

Synthesis of polyketone styrene (PKSt) and polyketone ether styrene (PKESt)

A solution containing (0.003 mol, 0.94 mg) ACSt monomer, with an equal mole of dialdehyde monomer (0.003 mol, 0.4 mg of terephthalaldehyde) or (0.003 mol, 0.97 mg of 4,4'-diformyl-α, ω -diphenoxyoctane) in 40 mL absolute ethanol, was stirred at 70° C until all reactants dissolved. The mixture was then treated with drops of 20% KOH (alcoh.) as a catalyst. The mixture was then stirred at the same temperature for 24 h. During this period, the solution's viscosity increased, the solution's color changed to a deep brown, and the polymer began to separate as the reaction progressed. The resultant polymer was filtered and washed with water, ethanol, and acetone before drying at 80 °C under reduced pressure for 24 h (1 mm/Hg). Elemental Anal. for (PKSt) $C_{27}H_{24}O_4$: Calcd. %: C, 78.62; H, 5.86. Found %: C, 78.25; H, 5.31 and for (PKESt) $C_{34}H_{30}O_6$: Calcd. %: C, 76.39; H, 5.66. Found %: C, 76.08; H, 5.15.

Results and discussion

PKs containing pendant styrene groups are highly desired for their possible usage in visible fluorescence emission. Two novel polymers, PKSt and PKESt, were synthesized via aldol reaction by polycondensation of DAcSt monomer with terephthaldehyde and previously prepared dialdehyde with aliphatic chain in its structure, using KOH as a catalyst.

The novel DAcSt monomer was prepared through an intramolecular aldol condensation and a Knoevenagel reaction by interacting cinnamaldehyde with acetylacetone in imidazole (a basic catalyst). The resulting DAcSt monomer is a six-membered ring with diacetyl groups and a pendant styrene group, as shown in Fig. 1. ^{1}H-NMR, ^{13}C-NMR, and FT-IR have demonstrated the structure of DAcSt. Figure S1 shows the ^{1}H-NMR spectrum of DAcSt in $CDCl_3$; the appeared signals correspond to the following: 5.22 ppm for (OH), 3.73–3.75 ppm for C_2H, 3.59–3.61 ppm for C_3H, 2.90–2.92 ppm for C_4H, 2.77–2.80 ppm for C_6H, 2.30–2.33 ppm for (C_6H), and 7.22—7.33 ppm for the aromatic ring. Figure S2 displays the ^{13}C-NMR spectrum of the carbon atoms' resonances with carbonyl groups is shown at 210.34, 206.36, and 205.63 ppm for (C_a = O), (C_b = O), and (C_c = O) correspondingly. The carbon atoms of aldehyde condensed with acetylacetone (-C_o–C=CH) are shown at 28.63 ppm, and the carbon atoms of aromatic

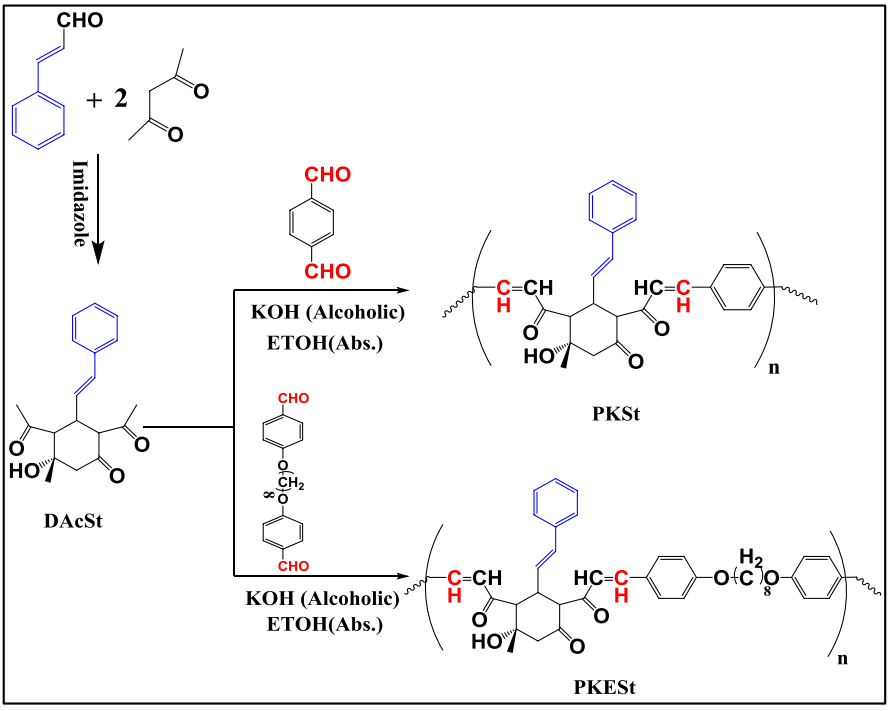

Fig. 1 Preparation of monomer (DAcSt) and polymers PKSt, PKESt

carbons appeared at 136.84, 129.17, and 129.12 ppm. The results obtained illustrate the success of monomer formation.

The FT-IR spectra of DAcSt monomer and polymers are shown in Fig. 2. The spectrum of DAcSt shows a peak at 3421 cm^{-1} strong and sharp peak, corresponding to the stretching vibration of the O–H group, 1719 cm^{-1} for the C=O stretching vibration, and 1694 cm^{-1} for the CH=CH of an alkene. The spectra of the resulting polymers reveal that the carbonyl groups, as a consequence of conjugation with C=C alkene bonds, are shifted to a lower wavenumber at 1693 cm^{-1} for PKSt and 1674 cm^{-1} for PKESt. Additionally, due to the extended conjugation, the C=C peaks move to a lower wavenumber, moving from (1694 in DACST to 1643 cm^{-1} in PKSt) and (to 1599 cm^{-1} in PKESt), respectively. In addition, the O–H group peaks in the PKSt and PKESt structures of the polymers are broader and moved to a lower wavenumber at 3408 and 3393 cm^{-1}, respectively; this could be because of intermolecular or extended hydrogen bonding. In addition, the PKESt comprises a long aliphatic chain and ether group; peaks at 2931–2851 and 1251 cm^{-1} identify the C–C and C–O ether group, respectively, and appear clearly in its spectrum. The polymers exhibit partial solubility in DMSO and DMF and are insoluble in ethanol, methanol, chloroform, or methylene chloride. This might be attributed to the presence of ketonic polar groups in their structures, which allows for partial dissolution in solvents that have similar properties.

According to Table 1 and Fig. 3a, the TGA curves of the polymer samples were studied using thermogravimetric analysis to determine how stable they were at high temperatures. The two polymers are degraded in three distinct phases. At

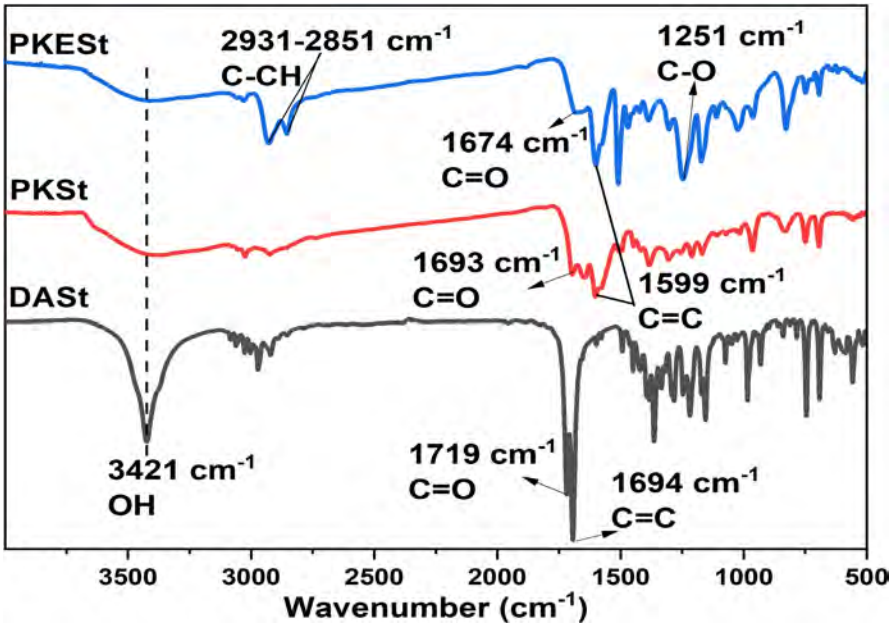

Fig. 2 FT-IR of DAcSt, PKSt, and PKESt

Table 1 Temperature (°C) for various decomposition levels in N_2 at a heating rate of 10 °C/min

Polymer	5% wt loss	10% wt loss	20% wt loss	30% wt loss	40% wt loss	50% wt loss	Char yield (%) at 650 °C
PKSt	157	294	394	477	549	663	51
PKESt	245	315	377	427	461	495	18

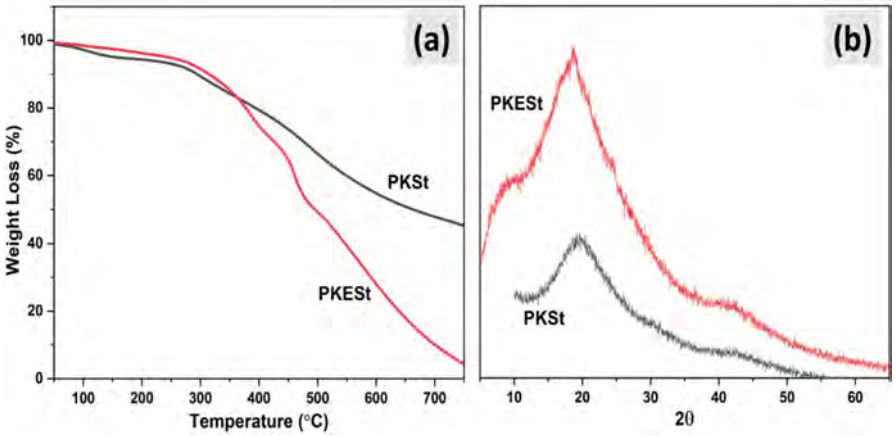

Fig. 3 **a** TGA curves. **b** X-ray graphs of PKSt and PKESt

temperatures below 250 °C, the PKESt's TGA thermogram reveals a little loss of mass (5% > weight loss) as a result of moisture and solvent vaporization. PKESt may tolerate temperatures up to 315 °C before experiencing a 10% weight loss owing to the breaking of intramolecular hydrogen bonding and the accompanying structure. The second rapid weight loss of 20%, which happens at 377 °C, is attributed to fragmentation and breaking of the molecular backbone and is quickly followed by the third degradation step at 450 °C. PKSt undergoes thermal degradation in the first phase at lower temperatures compared to PKESt, and the loss of moisture and solvents (< 5%) occurs at 157 °C. In three separate areas, the first stage is at 294 °C, which is thought to be caused by intermolecular hydrogen bonding breaking, and the second stage is at a temperature higher than 394 °C, which is caused by the polymeric backbone breaking down and also is followed quickly by the third stage at 470 °C [37]. PKSt exhibits a distinct thermal behavior in comparison with PKESt due to the significant occurrence of decomposition events at elevated temperatures (T > 380 °C) and greater residue at 650 °C (51% for PKSt, 18% for PKESt). The structure of PKSt, including aromatic moiety, differs from that of PKESt, which is based on an aliphatic chain; this structural difference accounts for the superior thermal stability of PKSt [38, 39].

The degree of crystallinity and other solid-state structural details are crucial features that may be obtained from X-ray diffraction (XRD) studies performed on polymer samples. The structural units of the produced polymers PKSt and PKESt

include aromatic rings, hydroxyl groups, ethylene bonds, and polar ketone groups in the monomeric units. The carbonyl group in the middle of the chain has a distinct orientation concerning the polymer. One key distinction is the presence of an aliphatic chain in PKESt, which may provide the chains with a certain amount of crystallinity and provide some flexibility [40]. The X-ray examinations of the prepared polymers are shown in Fig. 3b. PKSt has an amorphous structure caused by a lack of flexibility and aromatic ring packing without aliphatic chain separation, resulting in a broad peak. The inclusion of an aliphatic chain in the polymer backbone reduces chain packing and imparts some crystallinity, resulting in a lower amorphous structure in PKESt compared to PKSt. The increased β phase intensity in PKESt compared to PKSt suggests the existence of intermolecular hydrogen bonds due to the greater flexibility in PKESt. The degree of crystallinity of two polymers may be determined using the crystallinity index from XRD data, which can be derived from the area beneath the broad peak divided by the area of all peaks, including amorphous and crystalline ones. The degree of crystallinity of PKSt is around 38.7%, whereas that of PKESt is 42.5%. This suggests that both polymers are amorphous, but that PKESt is more crystalline than PKSt due to the presence of ether linkage and aliphatic chains [41, 42].

The uniform development of the polymer during polymerization is correlated with the systemic morphology of the polymers. The PKESt typically appears as clusters of spherical particles with a fuse at different magnifications and diameters ranging from 5 to 20 μm, as seen in Fig. 4a. The lack of a significant reduction in permeability with PKESt was because the chains were coiling owing to the intramolecular hydrogen bond and aliphatic chain within the polymer structure, preventing giant holes or fractures on the surface. The phase shown in Fig. 4b of PKSt was found to have aggregated clusters into rather large particles at higher magnification with diameters ranging from (20 to 50 μm) and the presence of a porous structure on the PKSt surface at smaller magnification with pores diameter (< 500 nm). The tightly packed aromatic rings in the polyketone chain structure, without separating by aliphatic chains, have caused the pore size to be formed and shape the surface-like membrane with a uniform distribution of pores throughout its surface [38]. The morphology shown in the scanning electron microscopy pictures indicates the creation of polymers, and the variation of the surface structure is due to the different ordering of the chains and molecules, which is caused by variations in the polymer's building components [43, 44].

Photophysical properties

Through the systematic use of UV–Vis absorption and fluorescence emission, the photophysical characteristics of DAcSt and polymers were investigated. The UV absorption spectra and the bandgap determined using Tauc's equation are shown in Fig. 5a and b. The DAcSt monomer samples and (PKSt, PKESt) polymers are examined in a DMSO solution, with DAcSt at concentrations ranging from (10^{-2} to 10^{-5} M), and each polymer is present in a concentration of 2 mg in 10 mL. As shown in Fig. 5a, the absorption spectra of DAcSt at various concentrations (ranging from

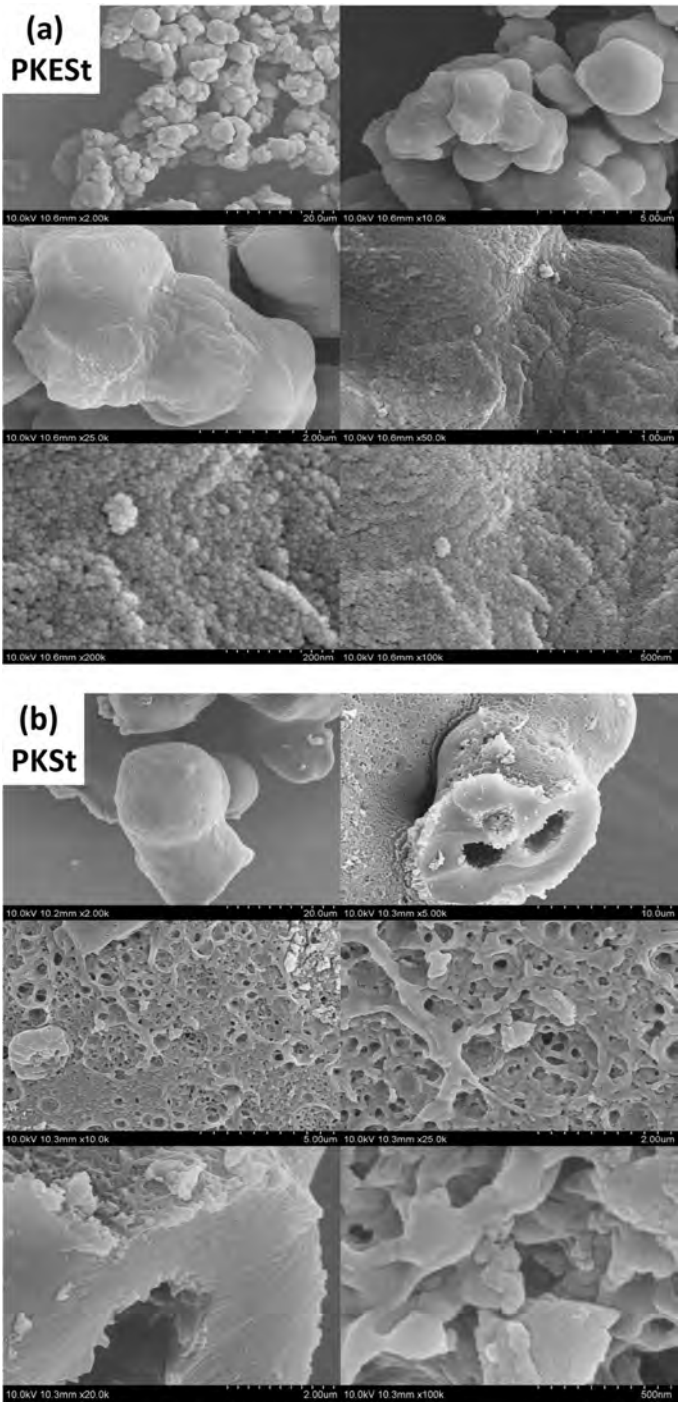

Fig. 4 SEM images at different magnifications for **a** PKESt and **b** PKSt

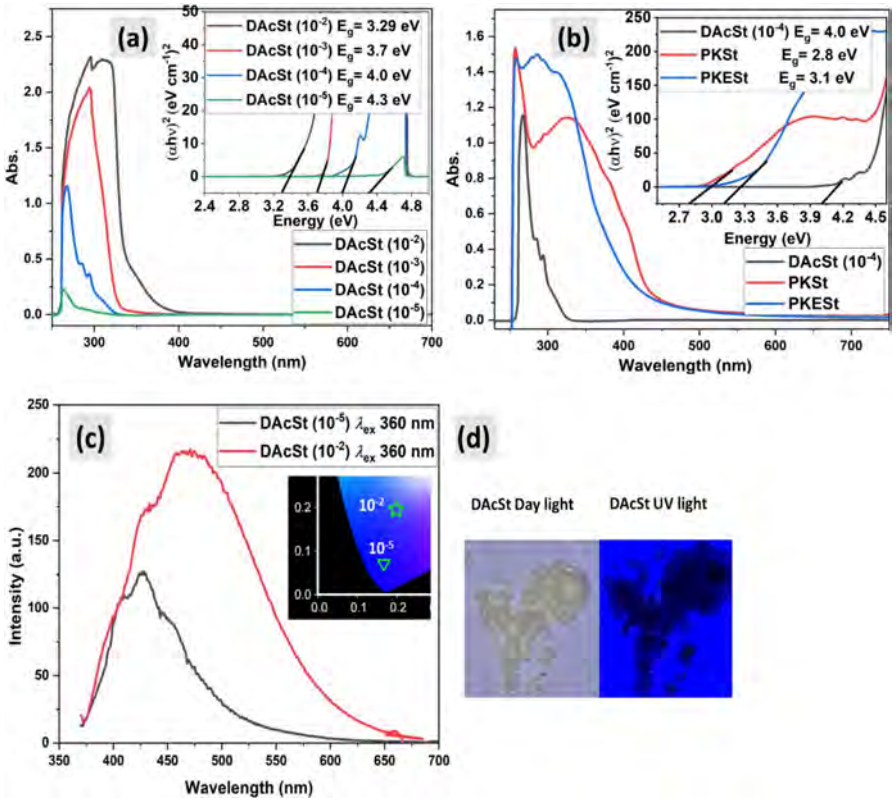

Fig. 5 **a** UV–visible absorption of DAcSt in different concentrations (10^{-2}- 10^{-5} M), inset Tauc`s plots of the samples. **b** UV–visible absorption of ($10^{-4}$ of DAcSt, 1 mg in 10 mL DMSO of polymers (PKSt, PKESt)), inset Tauc`s plots of them. **c** PL emission spectra of (10^{-2}, 10^{-5} M) DAcSt in DMSO at excitation (λ_{ex}= 360 nm), inset CIE diagram. **d** Images of solid DAcSt in day light and under UV light (λ_{ex}= 365 nm)

10^{-2} to 10^{-5} M) reveal that at a concentration of 10^{-2} M, the absorbance increases and two absorption peaks at 295 and 315 nm are noticed. One peak for lower concentrations at 293 nm for C=10^{-3}, at 267 nm for C=10^{-4}, and one at 263 nm for C=10^{-5} can be observed. The absorption peaks undergo a redshift as the solution concentration increases, and the longer peak either disappears entirely or changes into a little shoulder as the concentration reduces. As the concentration of monomer increases, the energy band gap also decreases; at C=10^{-2}, E_g= 3.29 eV, at C= 10^{-3}, E_g= 3.7 eV, C= 10^{-4}, E_g= 4.0 eV, and C= 10^{-5}, E_g= 4.3 eV. At larger concentrations, the π system and the (π-π) interaction between overlapping and parallel styrene are more prominent, which might cause additional absorption at longer wavelengths and a red shift in the absorbance band; this is why this result is seen. In a diluted solution, the solute molecules are widely spaced, preventing associative interaction and resulting in less absorption at longer wavelengths. Additionally, (π-π) interactions, dipole interactions, and hydrogen bonding are all more common at high

concentrations compared to low ones, and they may all contribute to a decrease in the molecule's band gap and an increase in aggregation.

Polymers have a UV absorption profile that is distinct from one another, depending on their structure. The PKSt has two distinct absorption peaks, one at 256 nm and the other at 325 nm; the second band is unique to the PKSt and distinguishes out. The presence of neighboring styrene units causes a rise in (π-π) contact, which in turn causes the larger absorption peak to appear. Three absorption peaks are seen in the PKESt: one at 256 nm, one at 287 nm, and one at 315 nm. The final peak shows a blue shift than the other polymer PKSt because the phenyl rings are isolated from each other through the aliphatic chains that are incorporated in its structure. As a result of the transition between the carbonyl group (n-π*) and the benzene ring (π-π*), it was discovered that the bandgap energy of the PKSt and PKESt groups reduced and reached around 2.8 eV and 3.1 eV, respectively [26]. Polymers exhibit a wide absorption band that reaches into the visible spectrum for both the (π-π*) aromatic and (n-π*) transitions. The blue shift of the small absorption peaks and lower-energy band gaps in highly diluted polymer solutions is caused by molecular aggregation and hydrogen bonding. This is observed clearly in PKSt, which has absorption that extends into the near UV. This is explained by the intramolecular interaction of hydrogen bonds within the unit structure and (π-π) interaction, which increases the wavelength absorption [45].

Figure 5c shows the photoluminescence (PL) spectra of DAcSt with the two concentrations (c $=10^{-2}$,10^{-5} M) obtained at the excitation wavelength (λ_{ex}) 360 nm. There was an emission peak of λ_{em} 427 nm for a concentration of 10^{-5} and an interesting red-shifted emission peak of λ_{em} 471 nm for the highly concentrated solution 10^{-2} at λ_{ex} 360 nm. The chromaticity diagram CIE and quantitative color coordinates (x, y) in Table 2 indicate their blue emission color according to their intensities. We deduced that the (PL) intensity increased as the concentration increased and the clusters formed in the concentrated solution must be the source of this emission. This is explained by the typical features of clusterization-triggered emission (CTE) [26, 46, 47]. In theory, the formation of clusters at low concentrations is improbable, and the PL intensity exhibits negligible variation due to the inherent difficulty of molecular interaction. The formation of clusters via enough intermolecular contacts

Table 2 Values of emission CIE coordinates of DAcSt, PKSt, and PKESt

Monomer	DAcSt 10^{-2}		DAcSt 10^{-5}
λ_{exc} 360 nm (x, y)	0.199, 0.196		0.170, 0.068
Polymer	λ_{exc} 256 nm (x, y)		λ_{exc} 325 nm (x, y)
PKSt (low c.)	0.222, 0.303		0.190, 0.171
PKSt (high c.)			0.196, 0.178
	λ_{exc} 256 nm (x, y)	λ_{exc} 287 nm (x, y)	λ_{exc} 315 nm (x, y)
PKESt (low c.)	0.193, 0.196	0.180, 0.156	0.175, 0.143
PKESt (high c.)			0.172, 0.125

occurred when the concentration was raised, and this resulted in a significant rise in PL intensity [48, 49].

As can be seen in Fig. 5b, PKESt's absorption spectrum revealed a very weak peak at around 315 nm, in contrast to PKSt's reasonably strong and broad absorption peak at 325 nm. Curiously, even though PKESt and PKSt had extremely similar absorbance peaks and emission characteristics, PKESt solution fluoresced blue color more strongly at 420 nm with CIE coordinates existed in Table 2 under different λ_{ex} values (256, 287, 325 nm) than PKSt solution did, and no excitation-dependent emission effect was observed for PKESt, Fig. 6a, b. Both polymers had a common PL characteristic, and PKESt solution had a better blue emission efficiency than PKSt, and they exhibited concentration-dependent PL spectra as shown in Fig. 6c, d. When the diluted PKSt solution (1 mg/10 mL DMSO) is excited at a wavelength of 325 nm, it exhibits (PL) with a relatively modest emission intensity and a more distinct peak compared to the concentrated solution (2 mg/10 mL DMSO). When a diluted solution of PKESt (1 mg/10 mL DMSO) is irradiated at a wavelength of 315 nm, a lower emission intensity is seen compared to the concentrated solution (2 mg/10 mL DMSO). Notably, the absorption intensity and the photoluminescence (PL) intensity both exhibit a linear increase with the concentration of PKSt and PKESt in the solution. The data above suggest that the AIE (aggregation-induced emission) property of polymers is independent of their polymer structure and may be attributed to their densely packed structure since polymer chains tend to collapse and aggregate at high concentrations.

According to photophysical characterization, PKESt's absorption and excitation spectra were almost identical to those of PKSt. Upon comparing the chemical structure of PKESt and PKSt, it was seen that the former had a more flexible polymer chain. Furthermore, under short wavelength UV light of 256 nm, PKESt even exhibited a bright blue emission, a feature that is rare in other systems. In contrast to PKESt, PKSt's PL spectra demonstrated an emission effect that was dependent on excitation, wherein the λ_{em} changed from white to blue as the λ_{ex} increased from 256 to 325 nm.

It has been shown that all of the CL-based materials are responsible for the light emission in these polymers since there are no traditional highly conjugated emission species. The key explanations for the distinct emission behaviors are the (CTE) mechanism of these nonconventional chromophores and the electron cloud overlapping to generate extended conjugation [19]. The blue emission in these CL-based materials was generated by the (n-π*) transition of the carbonyl group, and its strength was influenced by the electronic structure and conformational flexibility of the subunits. This is in line with previous research on the CL in carbonyl-based polymers, which found only oxygens with an abundance of electrons [50–52]. However, because of their relatively weak electron delocalization and conformability, isolated oxygen atoms produce weak emissions in solutions when subjected to visible light. In concentrated solutions and solids, on the other hand, these atoms may aggregate to create various clusters, with overlapping electron clouds. This provides molecules with longer conjugations, reduced energy gaps, and stiffened conformations. Furthermore, strong intramolecular and intermolecular interactions, as well as effective physical constraints between polymer chains, render these clustered chromophores

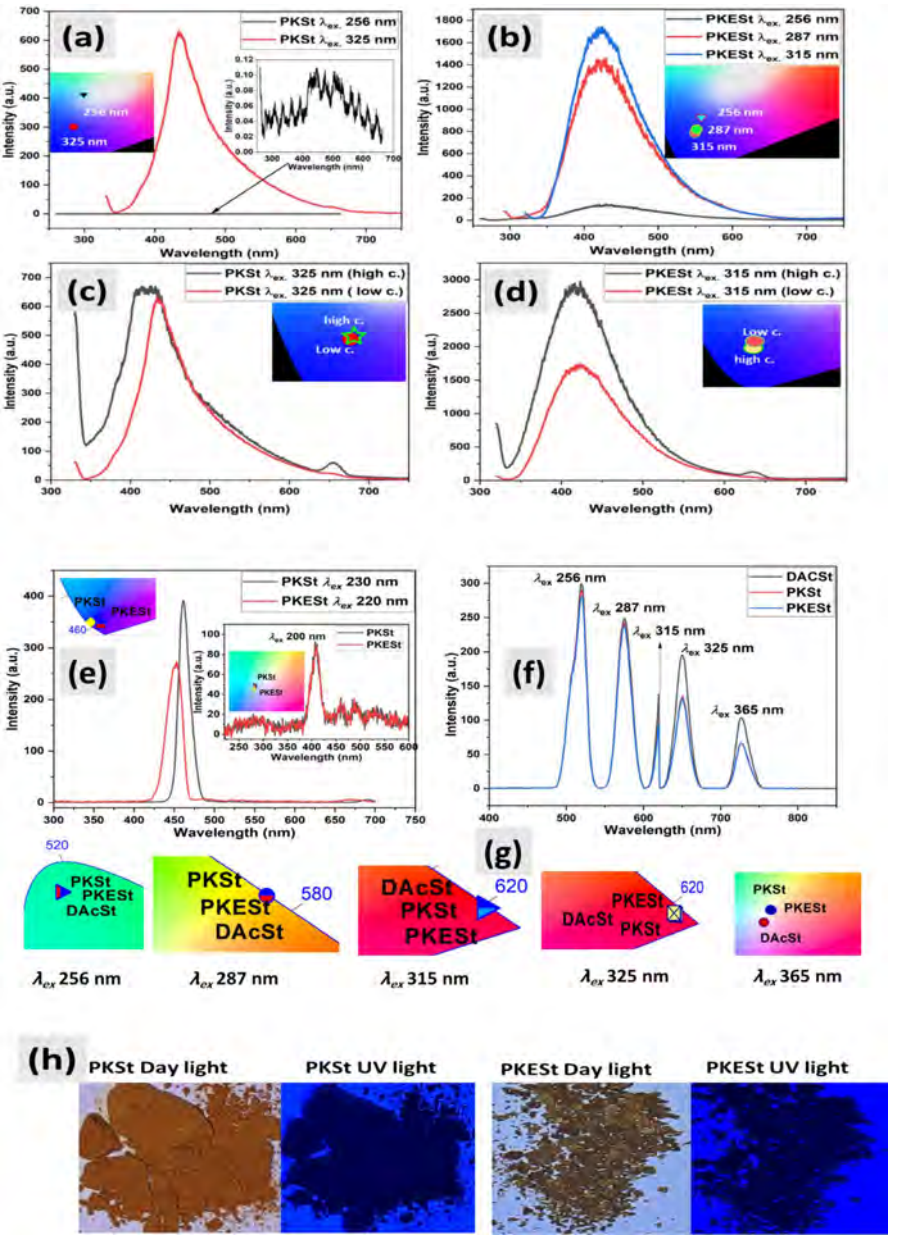

Fig. 6 **a** PL spectra of PKSt in DMSO at different excitation wavelengths (λ_{ex})(c = 1 mg in 10 mL). **b** PL spectra of PKESt in DMSO at different excitation wavelengths (λ_{ex})(c = 1 mg in 10 mL). **c** PL spectra of PKSt in DMSO at different concentrations (high c. = 2 mg/10 mL, low c. = 1 mg/10 mL) (λ_{ex} = 325 nm). **d** PL spectra of PKESt in DMSO at different concentrations (high c. = 2 mg/10 mL, low c. = 1 mg/10 mL) (λ_{ex} = 315 nm). Inset CIE diagram. **e** PL spectra of solid PKSt and PKESt at low excitation wavelengths (λ_{ex} = 220 nm) inset graph their emission at lower (λ_{ex} 200 nm). **f** PL spectra of solid DAcSt, PKSt, and PKESt at different excitation wavelengths (λ_{ex} = 256–365 nm). **g** CIE diagrams, **h** Images of solid PKSt and PKESt in daylight and under UV light (λ_{ex} = 365 nm)

suitable for excitation and deactivation via radiation. These constraints significantly rigidify the molecular conformations, thereby preventing nonradiative deactivations and enabling the emission of bright light [8]. Additionally, both C = C double bonds and OH groups play a significant role in producing luminescent species [53], (n-π*) transitions between heteroatoms and phenyls are another possible mechanism of interaction, and also, there is a potential that π electrons will result in π-π interactions. As a rule, strong CL-based materials are best achieved by using somewhat rigid polymer chains; adding aromatic rings to a polymer increases its backbone rigidity alters the molecules' amphipathic properties and boosts the clustering effect [54].

Since these polymers lack conjugation, the source of their emission is a significant abundance of oxygen atoms containing lone-pair electrons, as well as a nonconjugated π-system. Even though PKESt's chain is more flexible than PKSt's, and rigidness contributes to the emission's strength, PKESt contains more oxygen atoms than PKSt because of ether groups that boost the molecule's n-π^* transition and PL intensity [55].

The solid-state emission examination of the monomer and polymer samples is performed to investigate the AIE features, which is presented in Fig. 6e, f. The monomer has a greater solid-state emission than polymers owing to their simpler structure, which prevents tight packing.

In the solid state of PKST, PKEST, and DACST, excited wavelengths from 256 to 365 nm induced longer emission wavelengths toward the visible region than their solution, which can be attributed to more clustering leading to electronic transitions. In contrast to the solution state, molecules are often packed closer together in the solid state, which may result in stronger intermolecular interactions such as π-π stacking. These interactions increase the effective clustering, narrowing the energy gap between the HOMO and LUMO. This causes red-shifted emission at longer wavelengths. The AIE effect prevails, allowing aggregated molecules to emit longer wavelengths due to excimers or excitonic states. The molecule arrangement may improve π-orbital overlap, resulting in electronic state delocalization. Differences in polarity between solution and solid state may affect emission. The solid environment is less polar than usual solvents, changing excited-state stability and causing red-shifted emission. All of these causes move emissions into the visible range. At shorter wavelengths (< 315 nm), the monomer and polymer may have equal excited-state energy levels since the monomeric units' electronic structure dominates the emission. At these wavelengths, the prolonged clustering may not have a major impact on the emission from polymers; thus, we may get emissions that are very similar to those from monomers.

The polymers show enhanced aggregation at wavelengths exceeding 315 nm, resulting in a reduced HOMO–LUMO energy gap and allowing for emission at longer wavelengths. The lack of packing in the monomer indicates that minor molecular interactions, such as excimer formation or π-π stacking, are likely accountable for the enhanced wavelength emission. Efficient red-shifted emission may be achieved in the solid state of polymer chains by their formation of complex supramolecular structures such as aggregates, excimers, or J-aggregates. In addition, polymers are capable of self-absorption, which is the process by which neighboring

polymer chains reabsorb light that has been released. Longer wavelengths may so cause the observed emission to decrease. Energy moves either inside or across chains to aggregated or defect states—lower-energy emissive sites. This might lower the emission of more energetic waves; therefore, the polymer emits predominantly at longer wavelengths. Polymers' extended chains cause them to have stiffer structures, which might mean less room for nonradiative degradation routes. However, compared to the flexible monomer, this stiffness suggests that certain vibrational states may be inaccessible, which might slow down emission at higher wavelengths [56].

Compared to polymers, monomers have stronger emissions at longer wavelengths because they do not undergo energy transfer effects and keep their inherent emission properties. In this range, it may also show relatively greater emission due to its less complex structure and lower reabsorption tendency.

Clusteroluminogen emission intensity and color are susceptible to environmental factors such as temperature, viscosity, degree of dissolution, and pH, according to their mechanism of (CTE) [19]. Due to the abundance of atoms in CTE materials that possess a high electronegativity, these substances frequently adopt a light-emitting state after coordinating with metal ions and undergoing an aggregation transition. As a result, metal ion detection may be accomplished using them. The CTE may be used to detect changes in the amount of clustering caused by external factors, so many applications like monitoring, visualization, sensors, and probes exist in CL-based materials.

The Earth's crust contains a wide variety of heavy metals, some of which are essential for human health. These include iron (Fe), copper (Cu), cobalt (Co), magnesium (Mg), molybdenum (Mo), chromium (Cr), selenium (Se), manganese (Mn), nickel (Ni), and zinc (Zn). Nevertheless, these metals may harm humans if consumed in large quantities. Thus, it is crucial to develop materials that can identify these potentially harmful metals in food, water, and the environment [57]. Metals have been detected and categorized using colorimetric techniques for a long time because of their light-absorbing capabilities, which cause them to have rich and visually distinctive optical transitions [58]. When the metal interacts with a sensing moiety in a fluorescent material its fluorescence output varies upon contact with the analyte, fluorescent materials may be categorized as ratiometric change color, turn-off becomes less brilliant, or turn-on becomes more brilliant. Depending on whether the material undergoes a temporary or permanent alteration as a result of its contact with the metal, we may further categorize them as either reversible or reaction-based [59, 60].

To do this, one approach is to apply a chromogenic species specific to the metal of interest, helping to isolate the metal and providing a stronger signal compared to the background sample. For these chromogens to attach to metals and alter their structure visibly, they must have atoms with nonbonding electrons and double bonds [61, 62]. In these sensors, the excited material typically transfers electrons to the partly filled d-orbitals of the metal cations via the PET process [63].

The produced polymers PKSt and PKESt with clustering triggers exhibit unusual fluorescence activity, making them useful chemical tools for colorimetric detection of metal ions presence. Figure 7a-d and Table S1 depict the UV–Vis absorbance, fluorescence emission behavior, and CIE diagrams for PKSt and

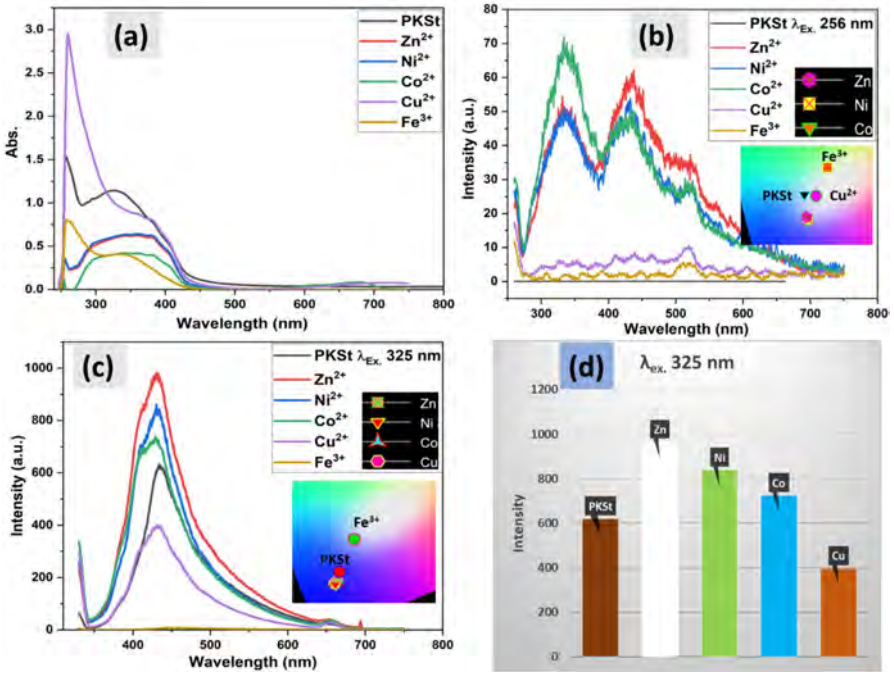

Fig. 7 **a** UV–visible absorption of PKSt in DMSO with different metal ions (Zn^{2+}, Ni^{2+}, Co^{2+}, Cu^{2+}, Fe^{3+}). **b** PL spectra of PKSt in (100 ppm) in DMSO with different metal ions (Zn^{2+}, Ni^{2+}, Co^{2+}, Cu^{2+}, Fe^{3+}) at (λ_{ex} = 256 nm), inset CIE diagram. **c** PL spectra of PKSt (100 ppm) in DMSO with different metal ions (Zn^{2+}, Ni^{2+}, Co^{2+}, Cu^{2+}, Fe^{3+}) at (λ_{ex} = 325 nm), inset CIE diagram. **d** Emission intensity of PKSt toward (Zn^{2+}, Ni^{2+}, Co^{2+}, Cu^{2+}, Fe^{3+}) at 325 nm

selected transition metal ions. The typical peaks of PKSt clusters occur at 256 nm, followed by a broad peak at 325 nm, according to its optical absorption spectrum. It has been discovered that the cluster's properties change when metal ions are added to the cluster solution, and these changes are ion-specific. In this study, the impact of metal ions on PKSt was investigated using 1 mg of transition metal ions (Zn^{2+}, Ni^{2+}, Co^{2+}, Cu^{2+}, Fe^{3+}) that were introduced to the cluster PKSt (100 ppm) DMSO. Upon the addition of Cu^{2+} and Fe^{3+} ions to the PKSt, the UV–Vis properties underwent a dramatic shift; a little redshift of the 256-nm absorbance peak was observed, along with a decrease in the widening of the 325-nm peak, Fig. 7a. For ions of (Zn^{2+}, Ni^{2+}, Co^{2+}) metal, the 256-nm peak was less intense, while the 325-nm peak was more prominent.

The fluorescence emission of PKSt at various excitation wavelengths in response to metal ion addition is displayed in Fig. 7b and c. At 256-nm excitation, Cu^{2+} and Fe^{3+} could generate an increase in white light emission fluorescence with a slight increase in emission intensity of PKSt solution. PKSt's color coordinates at 256-nm excitation shift from (0.222, 0.303) to (0.254, 0.301) with Cu^{2+} and to (0.286, 0.375) with Fe^{3+}. as a consequence of the presence of Zn^{2+}, Ni^{2+}, and Co^{2+} ions, the emission peak becomes somewhat more blue (blue shift),

which causes the solution's white light emission to decrease and shift toward blue light. At 256-nm excitation, the color coordinates shift to (0.229, 0.245) for Zn^{2+}, (0.233, 0.238) for Ni^{2+}, and (0.230, 0.237) for Co^{2+}. This change allows PKSt to differentiate between Cu^{2+} and Fe^{3+} ions from Zn^{2+}, Ni^{2+}, and Co^{2+} metal ions excited at the same wavelength. At 325-nm excitation, all these metals except the Fe^{3+} ion increase the emission intensity of PKSt solution resulting in deep blue light emission fluorescence (slight blue shift) as displayed in Fig. 7d. When Zn^{2+}, Ni^{2+}, Co^{2+}, and Cu^{2+} are added to PKSt solution, the color coordinates of PKSt at 325-nm excitation shift from (0.190, 0.171) to (0.188, 0.155), (0.180, 0.138), (0.182, 0.145), and (0.179, 0.141), respectively. Cu^{2+} ions increase the color but with a lower intensity than PKSt. In the presence of Fe^{3+} ions, the PKST solution's blue emission at 325-nm excitation becomes white, and a quenching of the intensity peak at color coordinates (0.227, 0.257) is observed. PKSt can readily differentiate Fe^{3+} from other metal ions at this excitation wavelength. Accordingly, at various excitation wavelengths, PKSt can detect Fe^{3+} from these metals with relative ease.

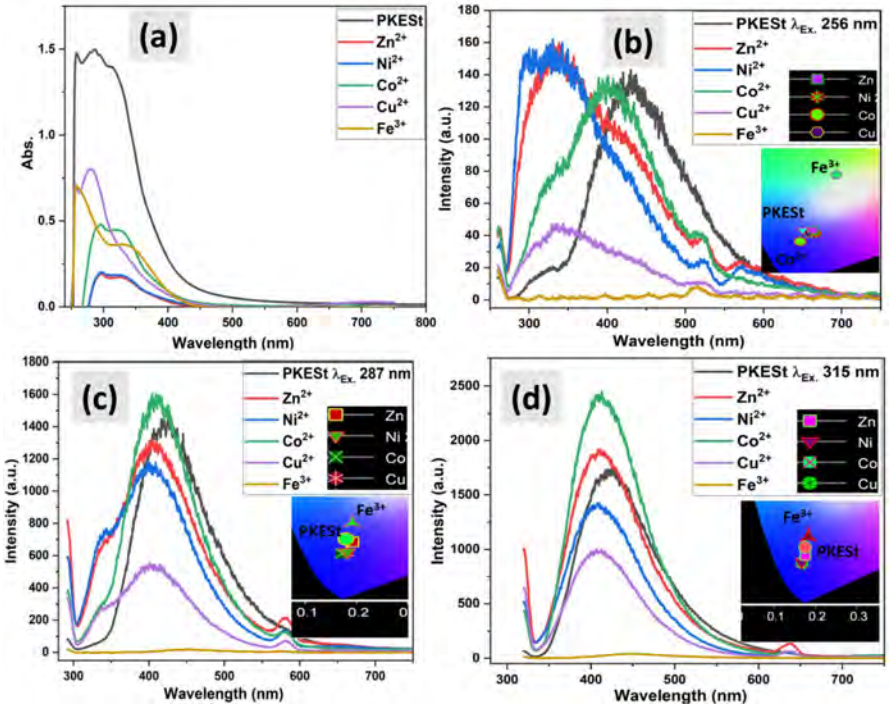

Fig. 8 **a** UV–visible absorption of PKESt in DMSO with different metal ions (Zn^{2+}, Ni^{2+}, Co^{2+}, Cu^{2+}, Fe^{3+}). **b** PL spectra of PKESt in (100 ppm) in DMSO with different metal ions (Zn^{2+}, Ni^{2+}, Co^{2+}, Cu^{2+}, Fe^{3+}) at (λ_{ex} = 256 nm), inset CIE diagram. **c** PL spectra of PKSt (100 ppm) in DMSO with different metal ions (Zn^{2+}, Ni^{2+}, Co^{2+}, Cu^{2+}, Fe^{3+}) at (λ_{ex} = 287 nm), inset CIE diagram. **d** PL spectra of PKESt (100 ppm) in DMSO with different metal ions (Zn^{2+}, Ni^{2+}, Co^{2+}, Cu^{2+}, Fe^{3+}) at (λ_{ex} = 315 nm), inset CIE diagram

Figure 8a–d and Table S1 show the optical characteristics of PKESt with the transition metal ions (Zn^{2+}, Ni^{2+}, Co^{2+}, Cu^{2+}, Fe^{3+}). The effect of adding these metals to the PKESt solution was also investigated using a cluster PKESt (100 ppm) DMSO solution that included 1 mg of these metal ions. As shown in Fig. 8a, the absorption behavior of PKESt changed when various metal ions were added to the solution. The addition of Zn^{2+}, Ni^{2+}, and Co^{2+} ions resulted in a notable phenomenon. These ions exhibited a redshift, a decrease in absorbance, and an expansion of the absorbance peak, leading to the emergence of a peak with two distinct regions. The addition of Cu^{2+} ions causes a blue shift and a shortening of the absorption peak, which makes the appearance of an obvious peak at 280 nm and a shoulder at 256 nm. The presence of Fe^{3+} ions produces a noticeable widening at 340 nm and a prominent 256-nm peak. The findings suggest that the apparent response to these metals is due to a cluster metal reaction resulting from a change in the electronic structure.

Figure 8b–d illustrates the fluorescence emissions of PKESt at various excitation wavelengths in response to metal ion addition. The excitation of the PKESt solution at 256 nm with the specified metal ions results in a blue shift in the PKESt emission peak from 429 nm (to 333 nm in Zn^{2+}, Ni^{2+}, Cu^{2+}) and 401 nm in Co^{2+} ions. As can be seen in the CIE coordinates from Table S1, the presence of Fe^{3+} ions in a PKESt solution causes white light fluorescence, shifting the coordinates from (0.193, 0.196) in PKESt to (0.281, 0.395) in the presence of Fe^{3+} ions. PKESt solution containing (Zn^{2+}, Ni^{2+}, Cu^{2+}) ions alters the emission color of the solution to purplish-blue according to their coordinates, which are (0.219, 0.196), (0.228, 0.184), and (0.211, 0.185), respectively. The presence of Co^{2+} in the PKESt solution causes a rise in blue emission fluorescence as its coordinates in CIE shift to (0.186, 0.156), accompanied by a reduction of emission intensity. A small blue shift occurs in the emission peak of the PKESt solution containing these various metal ions when it is excited at 287 or 315 nm. According to their CIE coordinates in Table S1 and Fig. 9, all metals produce blue light, but at varying intensities. The PKESt solution with Co^{2+} has the maximum intensity at 287- and 315-nm excitation wavelengths, while the solution with Fe^{3+} ions has the lowest intensity at the same excitation wavelengths. As a result of these findings, the PKEst solution may be used as a photocatalytic reagent in conjunction with Fe^{3+} at any of the other two excitation wavelengths or for ion selection at the 256-nm excitation wavelength. The PKESt and PKSt polymers' mechanism for metal ion sensing is based on fluorescence quenching or enhancement, coordination interactions, and charge transfer effects upon exposure to metal ions, Fig. 9c. The binding sites in polymers that coordinate with metals are carbonyl and ether groups capable of forming complexes. The optical and fluorescent properties of the polymer are also influenced by the electronic properties, which are altered by coordination. When energy is transferred from the polymer to the metal ion, a nonradiative degradation may result, or a nonfluorescent polymer–metal complex may form, causing quenching. The increase in fluorescence may result from diminishing nonradiative decay or preserving the excited state of the polymer. Structural stiffness induced by coordination may diminish internal vibrations and enhance fluorescence intensity. Certain metals may alter the electronic structure of polymers by facilitating Ligand-to-Metal Charge Transfer (LMCT) or Metal-to-Ligand Charge Transfer (MLCT), processes involving the transfer of charges from ligands to metals.

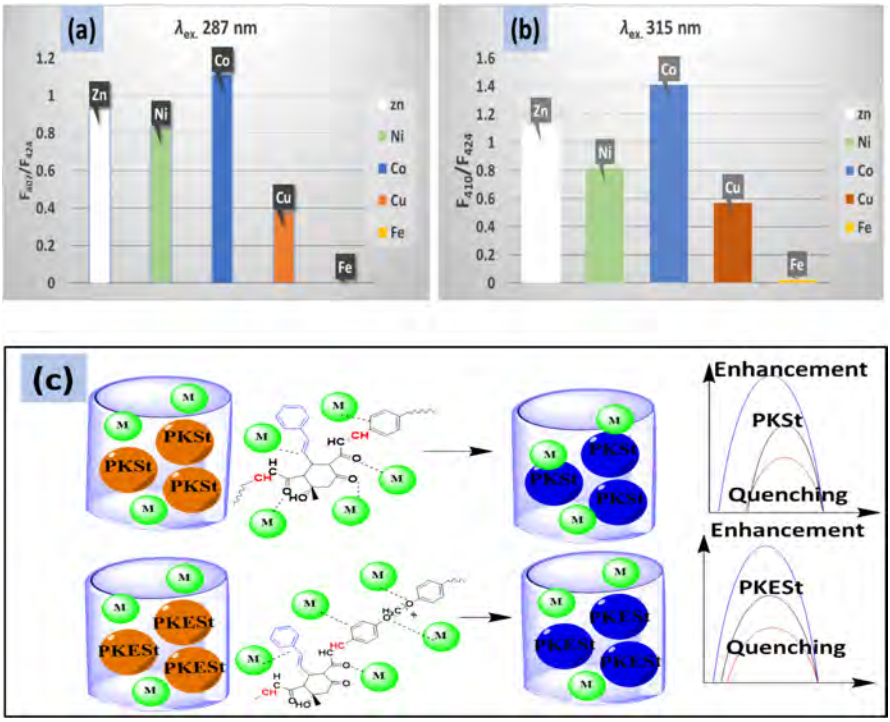

Fig. 9 Emission intensity ratio of PKESt with different metal ions (Zn^{2+}, Ni^{2+}, Co^{2+}, Cu^{2+}, Fe^{3+}). **a** At 407 and 424 nm. **b** At 410 and 424 nm. **c** Schematic diagram of metal ions sensing of PKSt and PKESt polymers

The selectivity and sensitivity of these polymers result from interactions involving ketone groups and aromatic rings [64].

Conclusion

In conclusion, this study successfully synthesized and characterized two novel fluorescent polyketones (PKs) that contain pendant styrene units. These polymers were identified as distinctive clustering-triggered emission (CTE) compounds and investigated through structural, thermal stability, and morphological analyses. The photophysical analysis showed that n-π*, π-π*, and hydrogen bonds cause PKESt and PKSt to display different luminescent behaviors and also aggregation-induced emission (AIE) features. Additionally, PKESt exhibited excitation-independent blue light emission, whereas PKSt exhibited excitation-dependent luminescence, emitting both white and blue light. These results contribute to the elucidation of clusteroluminescence (CL) mechanisms and propose new approaches for the development of innovative luminescent materials. Additionally, the exceptional selective fluorescence response of these PKs to Fe^{3+} ions and different responses for the selected transition

metals like (Zn^{2+}, Ni^{2+}, Co^{2+}, and Cu^{2+}), suggests their potential utilization as metal ion sensors. It may be possible to employ these polymers with Fe^{3+} as photocatalytic materials by taking advantage of the quenching effect that Fe^{3+} ions have on these Pks. This study not only provides new insights into the characteristics and uses of PKs clustering emission, but it also creates new opportunities for the creation of smart luminescent systems.

Supplementary Information The online version contains supplementary material available at https://doi.org/10.1007/s00289-025-05821-4.

Author contributions Marwa M. Sayed helped in conceptualization, writing—original draft, investigation. Islam S. Marae and Mohamed F. Mostafa contributed to investigation and visualization. Kamal I. Aly and Etify A. Bakhite helped in investigation and supervision.

Funding Open access funding provided by The Science, Technology & Innovation Funding Authority (STDF) in cooperation with The Egyptian Knowledge Bank (EKB).

Declarations

Competing interests The authors declare no competing interests.

Ethical approval and consent to participate Not applicable.

Consent for publication Not applicable.

References

1. Gao F, Liao Q, Xu Z-Z, Yue Y-H, Wang Q, Zhang H-L et al (2010) Strong two-photon excited fluorescence and stimulated emission from an organic single crystal of an oligo(phenylene vinylene). Angew Chem Int Ed 49(4):732–735
2. Samuel IDW, Turnbull GA (2007) Organic semiconductor lasers. Chem Rev 107(4):1272–1295
3. Li D, Zhang H, Wang Y (2013) Four-coordinate organoboron compounds for organic light-emitting diodes (OLEDs). Chem Soc Rev 42(21):8416–8433
4. Mishra A, Uhrich C, Reinold E, Pfeiffer M, Bäuerle P (2011) Synthesis and characterization of acceptor-substituted oligothiophenes for solar cell applications. Adv Energy Mater 1(2):265–273
5. Lou X, Zhang L, Qin J, Li Z (2008) An alternative approach to develop a highly sensitive and selective chemosensor for the colorimetric sensing of cyanide in water. Chem Commun 44:5848–5850
6. Li Q, Zhang WC, Wang CF, Chen S (2015) In situ access to fluorescent dual-component polymers towards optoelectronic devices via inhomogeneous biphase frontal polymerization. RSC Adv 5(124):102294–102299
7. Gong Y, Tan Y, Liu J, Lu P, Feng C, Yuan WZ et al (2013) Twisted D–π–A solid emitters: efficient emission and high contrast mechanochromism. Chem Commun 49(38):4009–4011

8. Zhang Yuan W, Zhang Y (2017) Nonconventional macromolecular luminogens with aggregation-induced emission characteristics. J Polym Sci, Part A: Polym Chem 55(4):560–574
9. Zhou Q, Cao B, Zhu C, Xu S, Gong Y, Yuan WZ et al (2016) Clustering-triggered emission of non-conjugated polyacrylonitrile. Small 12(47):6586–6592
10. Lu H, Feng L, Li S, Zhang J, Lu H, Feng S (2015) Unexpected strong blue photoluminescence produced from the aggregation of unconventional chromophores in novel siloxane–poly(amidoamine) dendrimers. Macromolecules 48(3):476–482
11. Yang L, Wang L, Cui C, Lei J, Zhang J (2016) Stöber strategy for synthesizing multifluorescent organosilica nanocrystals. Chem Commun 52(36):6154–6157
12. Gong Y, Tan Y, Mei J, Zhang Y, Yuan W, Zhang Y et al (2013) Room temperature phosphorescence from natural products: crystallization matters. Sci China Chem 56(9):1178–1182
13. Tomalia DA, Klajnert-Maculewicz B, Johnson KAM, Brinkman HF, Janaszewska A, Hedstrand DM (2019) Non-traditional intrinsic luminescence: inexplicable blue fluorescence observed for dendrimers, macromolecules and small molecular structures lacking traditional/conventional luminophores. Prog Polym Sci 90:35–117
14. Yang J, Fang M, Li Z (2020) Organic luminescent materials: The concentration on aggregates from aggregation-induced emission. Aggregate 1(1):6–18
15. Qin S, Zou H, Hai Y, You L (2022) Aggregation-induced emission luminogens and tunable multicolor polymer networks modulated by dynamic covalent chemistry. Chin Chem Lett 33(6):3267–3271
16. Yan J-J, Wang Z-K, Lin X-S, Hong C-Y, Liang H-J, Pan C-Y et al (2012) Polymerizing nonfluorescent monomers without incorporating any fluorescent agent produces strong fluorescent polymers. Adv Mater 24(41):5617–5624
17. del Mercato LL, Pompa PP, Maruccio G, Torre AD, Sabella S, Tamburro AM et al (2007) Charge transport and intrinsic fluorescence in amyloid-like fibrils. Proc Natl Acad Sci 104(46):18019–18024
18. Zhao E, Lam JWY, Meng L, Hong Y, Deng H, Bai G et al (2015) Poly[(maleic anhydride)-alt-(vinyl acetate)]: a pure oxygenic nonconjugated macromolecule with strong light emission and solvatochromic effect. Macromolecules 48(1):64–71
19. Zhang H, Zhao Z, McGonigal PR, Ye R, Liu S, Lam JWY et al (2020) Clusterization-triggered emission: uncommon luminescence from common materials. Mater Today 32:275–292
20. Tang S, Yang T, Zhao Z, Zhu T, Zhang Q, Hou W et al (2021) Nonconventional luminophores: characteristics, advancements and perspectives. Chem Soc Rev 50(22):12616–12655
21. Wang Z, Zhang H, Li S, Lei D, Zhong Tang B, Ye R (2022) Recent Advances in Clusteroluminescence. In: Tang Y, Tang BZ (eds) Aggregation-Induced Emission. Springer International Publishing, Cham, pp 43–64
22. Larson CL, Tucker SA (2001) Intrinsic fluorescence of carboxylate-terminated polyamido amine dendrimers. Appl Spectrosc 55(6):679–683
23. Dou X, Zhou Q, Chen X, Tan Y, He X, Lu P et al (2018) Clustering-triggered emission and persistent room temperature phosphorescence of sodium alginate. Biomacromol 19(6):2014–2022
24. Zhang H, Du L, Wang L, Liu J, Wan Q, Kwok RTK et al (2019) Visualization and manipulation of molecular motion in the solid state through photoinduced clusteroluminescence. J Phys Chem Lett 10(22):7077–7085
25. Zhang H, Tang BZ (2021) Through-space interactions in clusteroluminescence. JACS Au 1(11):1805–1814
26. Zhang H, Zheng X, Xie N, He Z, Liu J, Leung NLC et al (2017) Why do simple molecules with "isolated" phenyl rings emit visible light? J Am Chem Soc 139(45):16264–16272
27. Zhang J, Hu L, Zhang K, Liu J, Li X, Wang H et al (2021) How to manipulate through-space conjugation and clusteroluminescence of simple AIEgens with isolated phenyl rings. J Am Chem Soc 143(25):9565–9574
28. Shao S, Wang L (2020) Through-space charge transfer polymers for solution-processed organic light-emitting diodes. Aggregate 1(1):45–56
29. Jagt RBC, Gómez-Biagi RF, Nitz M (2009) Pattern-based recognition of heparin contaminants by an array of self-assembling fluorescent receptors. Angew Chem Int Ed 48(11):1995–1997
30. Yuen LH, Franzini RM, Wang S, Crisalli P, Singh V, Jiang W et al (2014) Pattern-based detection of toxic metals in surface water with DNA polyfluorophores. Angew Chem Int Ed 53(21):5361–5365
31. Pohl P (2009) Determination of metal content in honey by atomic absorption and emission spectrometries. TrAC, Trends Anal Chem 28(1):117–128

32. Karunasagar D, Arunachalam J (2001) Determination of cadmium by inductively coupled plasma mass spectrometry-reduction of molybdenum oxide interferences by addition of acetonitrile. Anal Chim Acta 441(2):291–296
33. Qiu L, Zhu C, Chen H, Hu M, He W, Guo Z (2014) A turn-on fluorescent Fe^{3+} sensor derived from an anthracene-bearing bisdiene macrocycle and its intracellular imaging application. Chem Commun 50(35):4631–4634
34. Aly KI, Elkhawaga AM, Hussein MA, Sayed MM (2013) Liquid crystalline polymers XI. Main chain thermotropic poly (arylidene–ether) s containing 4-methyl-cyclohexanone moiety linked with polymethylene spacers. Liquid Cryst 40(6):711–725
35. Aly KI, Sayed MM (2014) Liquid crystalline polymers XIV. Main chain thermotropic copoly (arylidene-ether) s based on 4-methyl-cyclohexanone and 4-tertiary-butyl-cyclohexanone moieties linked with polymethylene spacers. Liquid Cryst 41(1):67–81
36. Aly KI, Hussein MA, Sayed MM (2013) Liquid crystalline polymers XII. Main chain thermotropic poly (arylidene-ether) s containing 4-tertiary-butyl-cyclohexanone moiety linked with polymethylene spacers. Liquid Cryst 40(11):1570–1580
37. Alamry KA, Almehmadi SJ, Elfaky MA, Al-Shareef HF, Ja S, Hussein MA (2020) Enhanced antimicrobial activity of new arylidene-based polyketone nanocomposite materials. PolymerPlast Technol Mater 59(18):1973–1986
38. Jung YS, Canlier A, Hwang TS (2018) An efficient and facile method of grafting Allyl groups to chemically resistant polyketone membranes. Polymer 141:102–108
39. Aly KI, Abdel Monem MI (2005) New polymer synthesis. Synthesis and thermal behavior of new organometallic polyketones and copolyketones based on diferrocenylidenecycloheptanone. J Appl Polymer Sci 98(6):2394–2401
40. Sayed MM, Abd El-Hamid IS, El-Bery MH, Farrag M, Abdelhakiem AK, Aly KI (2022) Synthesis, characterization and application of high adsorption performance of novel 1, 4-polyketone. Sci Rep 12(1):16317
41. Sulcis R, Vizza F, Oberhauser W, Ciardelli F, Spiniello R, Dintcheva NT, Passaglia E (2014) Recycling ground tire rubber (GTR) scraps as high-impact filler of in situ produced polyketone matrix. Polymers Adv Technol 25(9):1060–1068
42. Ataollahi N, Girardi F, Cappelletto E, Vezzù K, Di Noto V, Scardi P, Callone E, Di Maggio R (2017) Chemical modification and structural rearrangements of polyketone-based polymer membrane. J Appl Polymer Sci 134(44):45485
43. Gonzales RR, Zhang L, Guan K, Park MJ, Phuntsho S, Abdel-Wahab A et al (2021) Aliphatic polyketone-based thin film composite membrane with mussel-inspired polydopamine intermediate layer for high performance osmotic power generation. Desalination 516:115222
44. Jia Y, Guan K, Zhang L, Lin Y, Shen Q, Zhang P et al (2021) Enabling polyketone membrane with underwater superoleophobicity via a hydrogel-based modification for high-efficiency oil-in-water emulsion separation. J Membr Sci 618:118705
45. Yang T, Li Y, Zhao Z, Yuan WZ (2023) Clustering-triggered phosphorescence of nonconventional luminophores. Sci China Chem 66(2):367–387
46. Zhang Y, He B, Luo W, Peng H, Chen S, Hu R et al (2016) Aggregation-enhanced emission and through-space conjugation of tetraarylethanes and folded tetraarylethenes. J Mater Chem C 4(39):9316–9324
47. Wang R-b, Yuan W-z, Zhu X-y (2015) Aggregation-induced emission of non-conjugated poly(amido amine)s: discovering, luminescent mechanism understanding and bioapplication. Chin J Polym Sci 33(5):680–687
48. Shen P, Zhuang Z, Jiang X-F, Li J, Yao S, Zhao Z et al (2019) Through-space conjugation: an effective strategy for stabilizing intramolecular charge-transfer states. J Phys Chem Lett 10(11):2648–2656
49. Chen L, Wang Y-H, He B, Nie H, Hu R, Huang F et al (2015) Multichannel conductance of folded single-molecule wires aided by through-space conjugation. Angew Chem Int Ed 54(14):4231–4235
50. Chu B, Zhang H, Hu L, Liu B, Zhang C, Zhang X et al (2022) Altering chain flexibility of aliphatic polyesters for yellow-green clusteroluminescence in 38% quantum yield. Angew Chem 134(6):e202114117
51. Zhang Z, Zhang Z, Zhang H, Sun JZ, Tang BZ (2022) The mysterious blue emission around 440 nm in carbonyl-based aliphatic clusteroluminogens. J Polym Sci 60(15):2127–2135
52. Zhang Z, Xiong Z, Chu B, Zhang Z, Xie Y, Wang L et al (2022) Manipulation of clusteroluminescence in carbonyl-based aliphatic polymers. Aggregate 3(6):e278

53. Niu S, Yan H, Chen Z, Yuan L, Liu T, Liu C (2016) Water-soluble blue fluorescence-emitting hyperbranched polysiloxanes simultaneously containing hydroxyl and primary amine groups. Macromol Rapid Commun 37(2):136–142
54. Zhang Z, Feng S, Zhang J (2016) Facile and efficient synthesis of carbosiloxane dendrimers via orthogonal click chemistry between Thiol and Ene. Macromol Rapid Commun 37(4):318–322
55. Miao X, Liu T, Zhang C, Geng X, Meng Y, Li X (2016) Fluorescent aliphatic hyperbranched polyether: chromophore-free and without any N and P atoms. Phys Chem Chem Phys 18(6):4295–4299
56. Chen X, Luo W, Ma H, Peng Q, Yuan WZ, Zhang Y (2018) Prevalent intrinsic emission from non-aromatic amino acids and poly(amino acids). Sci China Chem 61(3):351–359
57. Jaishankar M, Tseten T, Anbalagan N, Mathew BB, Beeregowda KN (2014) Toxicity, mechanism and health effects of some heavy metals. Interdiscip Toxicol 7(2):60–72
58. Carter KP, Young AM, Palmer AE (2014) Fluorescent sensors for measuring metal ions in living systems. Chem Rev 114(8):4564–4601
59. Zhang W, Luo Y, Yang M-X, Lin W-H, Redshaw C, Ni X-L et al (2022) Twisted cucurbit[14]uril: a new type of CTE macrocycle for Fe3+ sensing. Microchem J 178:107364
60. Rathinam B, Liu B-T, Nagarajan D, Kaliyamoorthy S (2023) Systematic analysis of colorimetric and fluorescent sensors for the detection of tin ions. J Taiwan Inst Chem Eng 147:104909
61. Huang J, Wang Y-L, Yu X-D, Zhou Y-N, Chu L-Q (2020) Enhanced fluorescence of carboxymethyl chitosan via metal ion complexation in both solution and hydrogel states. Int J Biol Macromol 152:50–56
62. Liao P, Huang J, Yan Y, Tang BZ (2021) Clusterization-triggered emission (CTE): one for all, all for one. Mater Chem Front 5(18):6693–6717
63. Tian X, Murfin LC, Wu L, Lewis SE, James TD (2021) Fluorescent small organic probes for biosensing. Chem Sci 12(10):3406–3426
64. Kaur B, Kaur N, Kumar S (2018) Colorimetric metal ion sensors – A comprehensive review of the years 2011–2016. Coord Chem Rev 358:13–69

Authors and Affil tions

Marwa M. Sayed[1] · Islam S. Marae[2] · Mohamed F. Mostafa[3] · Kamal I. Aly[4] · Etify A. Bakhite[2]

✉ Marwa M. Sayed
marwa.m@sci.nvu.edu.eg

✉ Kamal I. Aly
Kamalaly@aun.edu.eg

✉ Etify A. Bakhite
etafy@aun.edu.eg

[1] Chemistry Department, Faculty of Science, New Valley University, El-Kharja 72511, Egypt

[2] Department of Chemistry, Faculty of Science, Assiut University, Assiut 71516, Egypt

[3] School of Chemical Engineering, Yeungnam University, 280 Daehak-Ro, Gyeongsan, Gyeongbuk 38541, Republic of Korea

[4] Polymer Research Laboratory, Chemistry Department, Faculty of Science, Assiut University, Asyut 71516, Egypt